




Cite this: *RSC Adv.*, 2021, 11, 19673

Roles of solution concentration and shear rate in the shear-induced crystallization of P3HT†

Jiaxin He,‡ Ying Liu,‡ Fengquan Liu, Jianjun Zhou  and Hong Huo *

Microfluidic shear can induce the formation of flow-induced precursors (FIPs) of poly(3-hexylthiophene) (P3HT) in toluene. The shear temperature, solution concentration and shear rate determine the FIP content. The FIP is metastable. Upon fixing the shear rate at 1.0 s^{-1} and the shear temperature at 60°C (or 80°C for a 5.0 mg mL^{-1} solution), when the shear stress σ exceeds the critical values, a further increase in σ may destroy the formed FIP during shear, leading to the amount of FIPs first increasing when the solution concentration increases from 0.2 mg mL^{-1} to 0.4 mg mL^{-1} and then gradually decreasing with a further increase in the solution concentration from 0.7 mg mL^{-1} to 5.0 mg mL^{-1} . Upon fixing the shear temperature at 60°C (or 80°C for a 5.0 mg mL^{-1} solution), the high concentration P3HT solution has high viscosity, leading to more mechanical energy being dissipated under shear, resulting in the most suitable shear rate increases with increasing solution concentration to reduce the entropy. The reduction in entropy is related to the formation of FIPs, and thus, the most suitable shear rate at which the largest FIP content can be obtained increases with increasing solution concentration. The FIP content dramatically affects the crystallization of P3HT in toluene. Increasing the FIP content can accelerate nucleation and crystallization, and change the crystallization mechanism from a second-order reaction to a first-order reaction of P3HT aggregates.

Received 2nd April 2021
Accepted 10th May 2021

DOI: 10.1039/d1ra02594e

rsc.li/rsc-advances

Introduction

Conjugated polymers (CPs) represent a class of semiconducting materials with extensive applications in flexible optoelectronic devices, comprising organic photovoltaics, organic field-effect transistors, and polymer light-emitting diodes.^{1–3} For semi-crystalline CPs, in addition to the new chemical structure, properties such as the conjugation length, intermolecular coupling with crystalline aggregates, packing behaviour of the polymer chains, *etc.*, affect the applicable optic and electronic performance.^{4–6} Structural properties can be optimized by precisely modulating the crystallization process of the CPs. Processing approaches, including thermal annealing, solvent vapour annealing, solution processing, nanostructure confinement, the addition of nucleating agents, the use of rubbed or template substrates, and the addition of an external field (such as a magnetic field, ultrasonication, stretching and shear-coating), have been proven to be effective strategies for enhancing and controlling the nanoscale crystalline structure as well as intra- and intermolecular interactions of CPs and improving the charge transport performance.^{7–11}

Solution-based processability is an outstanding advantage of CPs. It is inevitable that CPs will experience a shear flow field during the solution process. The shear-induced crystallization of CPs has been a focus in recent years. Mackay *et al.* used a strain-controlled rheometer, Reichmanis *et al.* used a microfluidic shear method, and Egap *et al.* applied a shear coating method to process a poly(3-hexylthiophene) (P3HT) solution and found that the presence of shear improves the molecular order and charge transport characteristics of crystalline P3HT fibrils.^{12–15} However, few studies have investigated the molecular chain conformation transition, crystallization kinetics and crystallization mechanism of CPs under shear flow.

A fundamental understanding of shear-induced crystallization may help to tailor the ultimate properties of CPs. In a recent paper, we investigated the effects of microfluidic shear on the conformation transition and crystallization of P3HT in a dilute toluene solution.¹⁶ We found the absorption peak at 607 nm appears after the P3HT solution was shear at 60°C . The appearance of the absorption peak at 607 nm indicates that shear induces the polymer chains to shift from coil-like conformations to rod-like states, followed by π - π stacking of the rods. The peak at $\sim 607 \text{ nm}$ is often considered to originate from the interchain π - π transition of P3HT crystals. To justify the peak at 607 nm denote the flow-induced precursors (FIPs) or shear-induced crystals, we quenched the sheared solution (shear temperature is 60°C) to 16°C for isothermal crystallization. Because 16°C is a high temperature for P3HT

Beijing Key Laboratory of Energy Conversion and Storage Materials, College of Chemistry, Beijing Normal University, Xijiekouwai Street No. 19, Beijing 100875, P. R. China. E-mail: hhao@bnu.edu.cn

† Electronic supplementary information (ESI) available. See DOI: 10.1039/d1ra02594e

‡ Jiaxin He and Ying Liu contributed equally to this work.



crystallization in 0.2 mg mL^{-1} toluene solution, which has a relative long crystallization induction time for clearly observing the crystallization or relaxation of the shear-induced π - π stacked rods. In the sheared solution, if shear induces the formation of P3HT crystals at 60°C , then the crystallization may continue directly when the sheared solution is quenched to 16°C because the shear-induced crystals may supply a growth surface for subsequent crystallization. UV-vis spectra shows that the intensity of the absorbance peak at 607 nm in the sheared P3HT solution first decreases with isothermal time, indicating relaxation of the π - π stacked rods. Then, the intensity of the absorbance generally increases, indicating the crystallization of P3HT. The occurrence of crystallization after some relaxation of the π - π stacked rods suggests that the π - π stacked rods are not the nuclei or crystals of P3HT and that a rearrangement of the π - π stacking of the rods is necessary for the subsequent crystallization of P3HT, verifying that the shear-induced π - π stacked rods are mesomorphic; namely, they are FIPs, which are widely formed in sheared synthetic polymers (such as polyethylene (PE), poly(ethylene terephthalate) (PET), isotactic polypropylene (iPP) and isotactic polystyrene (iPS)^{17–19}) but were first observed in sheared CPs. The shear temperature (the temperature that the solution was kept when it was sheared) is an important parameter for determining the FIP content. The FIP content dramatically affects the crystallization kinetics, dispersion, content, and intrachain ordering of P3HT nanofibres when P3HT isothermally crystallizes at 12°C in toluene. In this article, we investigate the roles of the solution concentration and shear rate on the formation of FIPs and the crystallization of P3HT in toluene in detail. The results show that the shear temperature, shear rate and solution concentration determine the content of FIPs. The amount of FIPs dramatically affects the crystallization kinetics and crystallization mechanism of P3HT in toluene.

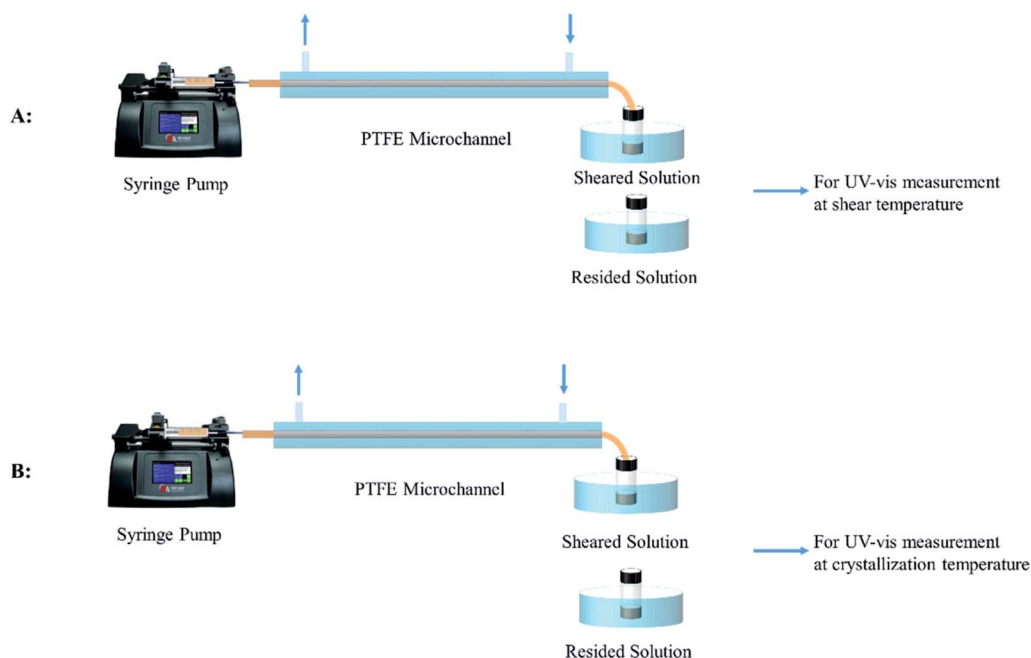
Experimental section

Materials

Poly(3-hexylthiophene) (P3HT) ($M_w = 5.8 \times 10^4 \text{ g mol}^{-1}$, polymer dispersity index (PDI) of 1.23, Rieke Metals Inc.) and toluene (Beijing Chemical Reagents Company) were used as received. P3HT solutions were prepared by dissolving the desired weight of P3HT in toluene at 90°C and stirring for 3 h. The concentrations of the P3HT solution were 0.2 mg mL^{-1} , 0.4 mg mL^{-1} , 0.7 mg mL^{-1} , 1.0 mg mL^{-1} and 5.0 mg mL^{-1} .

Microfluidic shear-induced crystallization of P3HT solutions

A syringe pump (D-401227, Harvard Apparatus) with a glass syringe (5 mL, 81520, Hamilton Company) was used to introduce the P3HT solution into the polytetrafluoroethylene (PTFE) microchannel (inner diameter: $300 \mu\text{m}$, outer diameter: $400 \mu\text{m}$, Shanghai Liangqi Fusu Inc.) to achieve microfluidic shear. The shear rate of the P3HT solution in the PTFE microchannel was controlled by setting the volumetric flow rate of the P3HT solution *via* an accurate syringe pump. The shear temperature was modulated by using a water bath surrounding the PTFE microchannel. The microfluidic shear method has been described in Scheme 1. The first step is to investigate the FIPs in the sheared solution, such as described as A process in Scheme 1. The P3HT solution was sheared and the sheared solution was collected into a quartz cuvette at the end of the PTFE microchannel and maintained at the shear temperature by using a water bath. The collection time was 30 s. The ultraviolet-visible (UV-vis) spectroscopy was measured at the temperature the same as the shear temperature. The UV-vis measurements at shear temperature was used to investigate the FIPs in the sheared solution. The second step is to investigate the effects of the FIPs on the crystallization kinetics of P3HT in the



Scheme 1 Experimental diagram of the microfluidic shear process.



sheared solution, such as shown as B process in Scheme 1. The shear and the collection process of P3HT solution (original solution) was repeated as in first step, after collected for 30 s at the shear temperature, the sheared P3HT solution was quenched to the isothermal crystallization temperature for the UV-vis spectroscopy measurement (the measurement temperature was set at the crystallization temperature in advance) to investigate crystallization kinetics of P3HT. Quiescent solution crystallization was performed for reference tests. The P3HT solution was held at the corresponding residence temperature for 30 s, and then, UV-vis measurements were performed, such as shown in Scheme 1. We denote the sheared solutions as $PS_{a,b}$ and the resided solutions as $PR_{a,b}$, where a is the solution concentration and b is the shear (or residence) temperature.

Characterization

An Agilent Cary 60 UV-vis spectrophotometer was used to record the solution and solid-state UV-vis spectra. The UV-vis absorbance of the P3HT solution was measured at wavelengths of $\lambda = 500\text{--}700$ nm. The UV-vis absorbance of P3HT films was measured at wavelengths of $\lambda = 300\text{--}700$ nm at room temperature. Grazing incidence X-ray diffraction (GIXRD) measurements were performed at 1W1A, Beijing Synchrotron Radiation Facility (BSRF), using a 9910 detector, a Si (220) single-crystal monochromator and a photon energy of 8.0049 keV. An incident angle of 0.1° was chosen to ensure probing of the samples. GIXRD images were normalized by the film thickness.

Results and discussion

Effect of the shear temperature on the solution crystallization kinetics

In our previous work, we verified that microfluidic shear can induce the formation of FIPs of P3HT in a toluene solution with a concentration of 0.2 mg mL^{-1} ($PS_{0.2}$), and the shear temperature has a great effect on the formation of FIPs. The formation mechanism of FIPs and the reason why the number of FIPs varied with the shear temperature were ascertained in detail. The FIP content dramatically affects the crystallization rate of P3HT at 12°C in toluene.¹⁵ Here, we studied the microfluidic shear-induced crystallization kinetics of $PS_{0.2}$ at different crystallization temperatures in detail by using *in situ* UV-vis spectroscopy. It is known that the residence temperature has no effects on the crystallization rates of $PR_{0.2}$,¹⁶ and thus, a residence temperature of 60°C was chosen for the resided solutions. Some research groups have reported that shear temperatures above the equilibrium melting temperature change the features of FIPs, further affecting the crystallization morphology and crystallization rate of polymers in the melt.^{20–23} In this work, we studied the effects of FIPs on the crystallization of P3HT in solution, and the equilibrium dissolution temperature T_d^0 needs to be evaluated to determine a suitable shear temperature. The Hoffman–Weeks method was used to measure the T_d^0 of P3HT toluene solution.²⁴ The P3HT solution was held at the reset crystallization temperature (T_c) for 24 h for isothermal crystallization. Then the isothermally crystallized P3HT was heated with $10^\circ\text{C min}^{-1}$ to dissolve the produced crystals. The dissolution process was monitored by

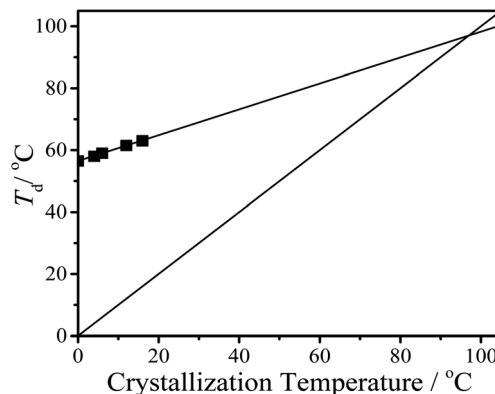


Fig. 1 Dissolution temperature (T_d) of P3HT in toluene as a function of the isothermal crystallization temperature (T_c). The data are linearly extrapolated to the line of $T_d = T_c$ to obtain T_d^0 at the intersection point. The concentration of P3HT solution is 0.2 mg mL^{-1} .

UV-vis spectroscopy to determine the dissolution temperature (T_d). The absorption intensity at ~ 607 nm decreased with the increase of the solution temperature, the temperature at which the absorption peak at ~ 607 nm disappeared was T_d . The data were plotted as T_d versus T_c , as shown in Fig. 1. The diagonal line in Fig. 1 represents $T_d = T_c$. The data of T_d versus T_c were then linearly extrapolated to an intersection, T_d^0 , on the diagonal line. The T_d^0 value of pure P3HT in toluene was calculated to be 96°C , which is similar to that of P3HT crystallization in anisole.²⁴ Shear temperatures of 20°C and 60°C (both below T_d^0) were chosen to investigate the effects of shear (or the FIP content) on the crystallization kinetics of $PS_{0.2}$. The isothermal crystallization temperatures were 6°C , 8°C , 10°C and 12°C . The continued increase in the intensity of the absorption peak at ~ 607 nm indicates the crystallization and aggregation of P3HT in solution.^{24–26} The absorption peak at ~ 607 nm was used to monitor the crystallization of P3HT in toluene *in situ*, the same as that in previous work.¹⁶ Fig. S1† shows that the absorbance at $\lambda \sim 607$ nm varied with time for $PR_{0.2,60}$, $PS_{0.2,20}$ and $PS_{0.2,60}$ crystallized at different temperatures. The initial rate method was used to evaluate the growth rate of P3HT crystals (G), and the results are summarized in Fig. 2. As

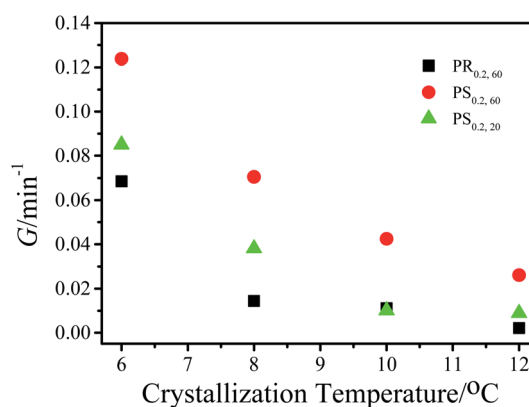


Fig. 2 Plots of the growth rate of P3HT crystals (G) versus the isothermal crystallization temperature of $PR_{0.2,60}$, $PS_{0.2,20}$ and $PS_{0.2,60}$. The shear rate is 1.0 s^{-1} .



expected, decreasing the crystallization temperature resulted in the coil-to-rod transition to minimize the total free energy and thereafter accelerated the crystallization of P3HT. At the same crystallization temperature, imposing shear on the P3HT solution significantly increased G . G was higher for the P3HT solution sheared at 60 °C than for the solution sheared at 20 °C.

The acceleration of shear-induced crystallization kinetics is an apparent change compared with that of quiescent crystallization. Such enhanced crystallization kinetics are mainly attributed to the significantly increased nucleus density and growth rate, namely, the shear flow would eventually lead to an increased nucleation rate once the shear rate exceeds a critical value.^{21,27} Under shear, polymer chains aligned along the shear direction, reducing the entropy due to fewer possible chain configurations. From a thermodynamic point of view, Flory proposed that the reduction in entropy lowers the nucleation energy barrier (ΔG_n^*), resulting in nucleation acceleration.^{28,29} Hoffman and Lauritzen proposed that the nucleation barrier under quiescent conditions is expressed as³⁰

$$\Delta G_{n,q}^* = (2ab\sigma_e + 2a\sigma_s + 2bl\sigma_s) - V^*(T_c)\Delta f(T_c) \quad (1)$$

where $(2ab\sigma_e + 2a\sigma_s + 2bl\sigma_s)$ is the total interfacial energy of a nucleus created with dimensions a , b , and l with lateral surface energy σ_s and end surface energy σ_e . $V^*(T_c)$ is the critical nucleus volume, and $\Delta f(T_c)$ is the enthalpy difference between the amorphous and crystalline phases per unit volume at the crystallization temperature T_c . McHugh proposed that the mechanical work applied to polymers can decrease $\Delta G_{n,s}^*$ due to entropy reduction as³¹

$$\Delta G_{n,s}^* = (2ab\sigma_e + 2a\sigma_s + 2bl\sigma_s) - V^*(T_c)\{\Delta f(T_c) - T_s\Delta S\} \quad (2)$$

where T_s is the shear temperature and ΔS is the entropy reduction per unit volume by shear ($\Delta S < 0$). Under shear, the random coil chains of P3HT experience a transition from coil to rod in the solution, and these rigid rods start the isotropic-nematic transition to form a locally anisotropic structure. Then, rod bundles are formed as FIPs for the nucleation and growth of P3HT.^{16,21} The formation mechanism of FIP indicates that the reduction in entropy increases with increasing FIP. The amount of FIP formed at 60 °C is higher than that at 20 °C,¹⁶ and the T_s at 60 °C is higher than that at 20 °C; therefore, the value of $-T_s\Delta S$ sheared at 60 °C is higher than that at 20 °C, resulting in a decrease in $\Delta G_{n,s}^*$, and thus, the nucleation (or crystallization) rate at a high shear temperature of 60 °C is higher than that at 20 °C.

Effect of the solution concentration on the shear-induced crystallization of P3HT in toluene

The formation of FIPs indicates that shear induces the coil-to-rod transition of P3HT chains in a toluene solution. When the concentration of the rods exceeds a threshold, π - π stacking of the rods spontaneously occurs to form FIPs. This infers that the solution concentration may greatly affect the number of shear-induced rods, followed by FIPs. In polymer solution, when the concentration reaches a critical semidilute solution concentration (c^*), the molecular chains begin to contact. When the solution concentration further increases, the molecular chains

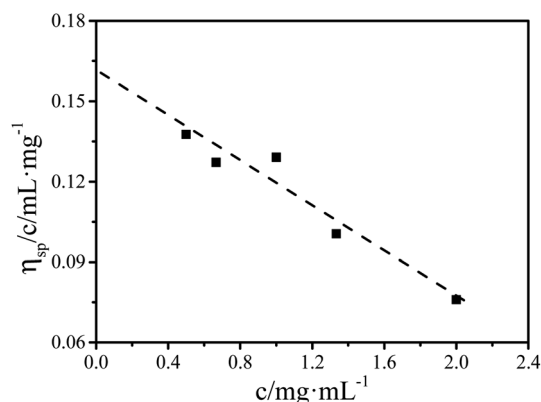


Fig. 3 Variation in the reduced viscosity η_{sp}/c and the solution concentration c of P3HT toluene solutions.

entangle with each other, which hinders molecular motion and restricts the conformation transition. The shear-induced crystallization for dilute solutions can be described by the coil-stretch transition model, and for highly entangled polymers, the stretched network model is used.²¹ An Ubbelohde viscometer was used to measure the c^* of P3HT toluene solution at 25 °C. Fig. 3 shows that the reduced viscosity (η_{sp}/c) linearly varies with the solution concentration (c), and the extrapolated intercept at $c = 0$ is the specific viscosity ($[\eta]$), 0.16 mL mg⁻¹. Meanwhile, c^* is the reciprocal of $[\eta]$, and the value is 6.3 mg mL⁻¹. In this work, the concentrations of P3HT toluene solutions were below 5.0 mg mL⁻¹, and they were all dilute solutions. P3HT molecular chains have no entanglements in dilute toluene solutions.

Fig. 4a shows the UV-vis spectra of PS_{0.7} sheared at different temperatures. There is an obvious absorption peak at ~607 nm in each spectrum, indicating that shear induced a coil-to-rod transition and that the rods underwent π - π stacking to form FIPs at each shear temperature. The intensity of the absorption peak at ~607 nm increased as the shear temperature increased from 12 °C to 60 °C and decreased slightly with further increases in the shear temperature to 80 °C. This result is similar to that of PS_{0.2}.¹⁶ Fig. 4b shows the UV-vis spectra of PS_{5.0} sheared at different temperatures. PS_{5.0} began to crystallize before the sheared solution was completely collected (~30 s) for UV-vis measurement when the solution was sheared at 12 °C, and the absorption intensity was above the measurement limitation for UV-vis spectroscopy after the solution was collected, such as shown in Fig. S2.† Thus, the shear temperature was varied from 20 °C to 80 °C. No obvious absorption peak was observed when the shear temperature was below 40 °C, indicating that no FIPs formed in these sheared solutions. The absorption peak at ~607 nm appeared when the solution was sheared at 60 °C, and the intensity increased slightly with the elevation of the shear temperature, verifying that a few FIPs formed when the shear temperature was above 60 °C and that the FIP content was slightly larger in the solution sheared at 80 °C than in the solution sheared at 60 °C. The UV-vis spectra of the corresponding resided solutions are shown in Fig. S3.† No absorption peaks appear in each resided solution, indicating



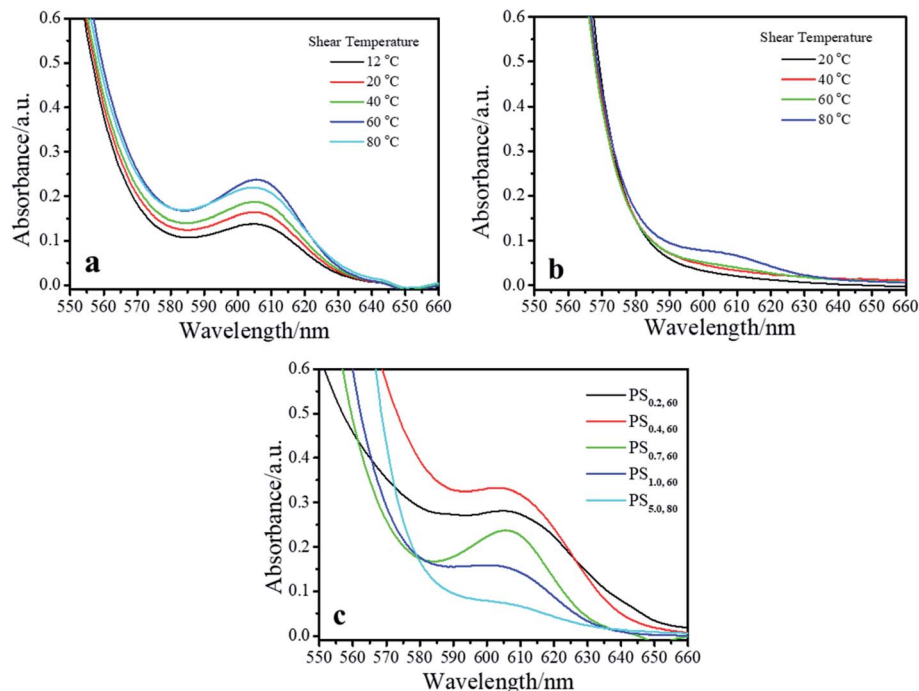


Fig. 4 UV-vis absorption spectra of (a) PS_{0.7} and (b) PS_{5.0} sheared at different temperatures. (c) UV-vis absorption spectra of sheared P3HT solutions with different concentrations. The shear temperature of PS_{5.0} is 80 °C, and the shear temperature of the other solutions is 60 °C. The shear rate is 1.0 s⁻¹.

that no FIPs form in PR_{0.7} and PR_{5.0} at different residence temperatures. Fig. 4c shows UV-vis absorption spectra of sheared P3HT solutions with different concentrations. To maximize the absorption intensity of the peak at ~607 nm for each P3HT solution, we choose a shear temperature of 80 °C for PS_{5.0} and a shear temperature of 60 °C for the other solutions. As shown in Fig. 4c, the peak intensity increased when the solution concentration increased from 0.2 mg mL⁻¹ to 0.4 mg mL⁻¹, and then, the peak intensity gradually decreased with a further increase in the solution concentration from 0.7 mg mL⁻¹ to 5.0 mg mL⁻¹.

The effects of shear flow on the formation of FIPs are determined by external flow parameters, such as the shear rate $\dot{\gamma}$, shear time t_s , shear strain γ and shear stress σ .^{32,33} The shear strain $\gamma = \dot{\gamma} \times t_s$ and the shear stress $\sigma = \eta(\dot{\gamma}) \times \dot{\gamma}$, where $\eta(\dot{\gamma})$ is the solution viscosity at $\dot{\gamma}$. σ can create metastable flow-induced clusters, while γ can enhance the frequency of collisions to transform the metastable cluster into a stable nucleus.^{32,34,35} The shear stress σ is the key parameter to determine the formation of metastable flow-induced clusters, namely, FIPs. In Fig. 4, $\dot{\gamma}$ and t_s are fixed, resulting in the shear strain γ being a fixed value. The solution viscosity increases with the solution concentration, resulting in the shear stress σ being higher in P3HT solutions with higher concentrations. The FIP is metastable; when the shear stress σ exceeds the critical values, a further increase in σ may destroy the formed FIP during shear, leading to the amount of FIPs first increasing when the solution concentration increases from 0.2 mg mL⁻¹ to 0.4 mg mL⁻¹ and then gradually decreasing with a further increase in the solution concentration from 0.7 mg mL⁻¹ to 5.0 mg mL⁻¹. Cui *et al.*

reported similar experimental phenomena. They investigated the flow-induced crystallization of bimodal poly(ethylene oxide) blends and found that the FIP was destroyed by further increasing the flow intensity, leading to an increased onset time of crystallization and low orientation of initial lamellar crystals under a large shear intensity.³⁶ In the same way, when the solution concentration was fixed at 5.0 mg mL⁻¹, as shown in Fig. 4b, the solution viscosity decreased with increasing solution temperature, resulting in the shear stress σ decreasing with increasing shear temperature, fewer FIPs were destroyed and the number of FIPs increased with increasing shear temperature. In the solution with a concentration of 0.7 mg mL⁻¹, the solution viscosity was low, and the variation in the solution viscosity with temperature was small, resulting in the destruction of the FIPs by shear being relatively faint. The variation trend and the formation mechanism of FIPs with shear temperature in the 0.7 mg mL⁻¹ solution are similar to those in the 0.2 mg mL⁻¹ solution.¹⁶

The effects of shear on the crystallization kinetics of different concentrations of P3HT in toluene were investigated by using UV-vis spectroscopy. No FIPs formed in each resided solution with different concentrations and different residence temperatures. It was speculated that the residence temperature has no effect on the crystallization rate of P3HT solutions with different concentrations. To verify this hypothesis, we chose PR_{0.7} as a representative solution with a high concentration. Fig. S4† shows that the crystallization rates of P3HT in PR_{0.7} are similar, verifying that the residence temperature had no effects on the crystallization of P3HT in toluene, which is the same as the results for PR_{0.2}. In PS_{5.0}, the absorption peak intensity was



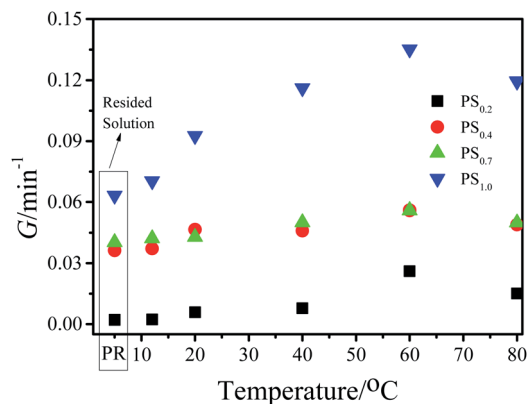


Fig. 5 Effects of the shear temperature on the crystallization rate of P3HT in toluene at different concentrations. The isothermal crystallization temperature is 12 °C, and the shear rate is 1.0 s⁻¹.

above the measurement limitation for UV-vis spectroscopy when P3HT was crystallized at 12 °C, and thus, no crystallization kinetics data were obtained. Theoretically, the concentration dependence of the crystallization rate at a constant temperature is expressed as:³⁷

$$G = kc^\alpha \quad (3)$$

where k is the rate constant and α is the reaction order. α is solely associated with the reaction mechanism. To evaluate α , the crystallization rates of P3HT in PS_{0.2}, PS_{0.4}, PR_{0.7} and PS_{1.0} were obtained by using the *in situ* UV-vis method. Since the residence temperature had nearly no effect on G in the resided solutions, we used the G of P3HT with a residence temperature of 60 °C to represent the crystallization rate of P3HT in the resided solutions. The values of G in the resided solutions and sheared solutions are summarized in Fig. 5. The results show that G of the sheared solution was higher than that of the resided solution at each concentration, verifying that shear accelerates the crystallization of P3HT in toluene. In the sheared solution with the desired concentration, G increased as

the shear temperature increased from 12 °C to 60 °C and then decreased slightly with further increases in the shear temperature to 80 °C, indicating that the effects of shear on the crystallization of P3HT in toluene with concentrations between 0.2 mg mL⁻¹ and 1.0 mg mL⁻¹ were similar. Since the crystallization rate of P3HT differs greatly in toluene with different concentrations, it is difficult to choose a suitable isothermal crystallization temperature other than 12 °C.

The plots of $\ln G$ versus $\ln[P3HT]$ are shown in Fig. 6a. The data show that P3HT sheared at the same shear temperature falls onto the best fit straight lines, and the slopes of the straight lines determine the reaction order α . α is 2.12 for P3HT crystallized in the resided solution. As the shear temperature increases from 12 °C to 80 °C, α is 2.07, 1.52, 1.41, 0.69 and 1.01. Our data indicate that variation in the shear temperature changes the value of the reaction order α and thus changes the crystallization mechanism of P3HT in toluene. During quiescent crystallization in the resided solution, α was approximately 2, and aggregation and crystallization were second-order reaction. In the sheared solution, the aggregation and crystallization processes generally changed from second-order reaction to first-order reaction as the shear temperature increased from 12 °C to 80 °C. The above results indicate that the FIP content affected the crystallization mechanism of P3HT in sheared toluene solutions. At high shear temperatures, the FIP content is large, and the crystallization of P3HT tends to be a first-order reaction. At low shear temperatures, the FIP content was low, and the crystallization of P3HT tended to be a second-order reaction. The shear-induced solution crystallization of P3HT in a marginal solvent underwent a coil-to-rod conformational transition, π - π stacking of the rods to form FIPs and then nucleation and crystallization. In summary, it includes two processes: a coil-to-rod transition and π - π stacking of the rods. For the coil-to-rod transition, Zhang's group showed inverse first-order kinetics behaviour.^{38,39} For rod-rod aggregation, scaling establishes a nucleation rate proportional to the concentration raised to the second power.⁴⁰ Therefore, the overall reaction order of P3HT crystallization is determined by the relative contributions of each process. Currently, there are

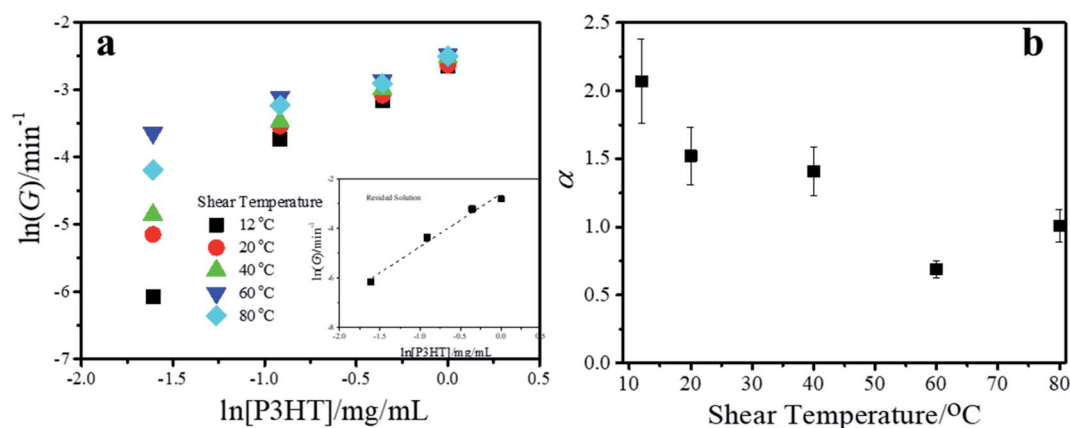


Fig. 6 (a) Plots of $\ln G$ versus $\ln[P3HT]$ at different shear temperatures. The inset shows a plot of $\ln G$ versus $\ln[P3HT]$ of the resided solutions, and the residence temperature is fixed at 60 °C. (b) Variations in α with the shear temperature.



no effective ways to either predict or measure the weighting factor of each process. In this work, in the resided and sheared solutions at low temperature, α was approximately 2, indicating that the rod aggregation process may contribute more. With the elevation of the shear temperature and the coil-to-rod transition strengths, more FIPs form, and α decreases to a value below 1, indicating that the coil-to-rod transition process becomes dominant.

GIXRD was used to investigate the crystalline structures of shear-induced P3HT aggregates formed in solutions with different concentrations. As shown in Fig. S5a and b,[†] all P3HT aggregates show a (100) plane at $2\theta = 5.5^\circ$, indicating that the orientation of the P3HT crystal planes in these samples is primarily edge-on, and the shear temperature has no effect on the crystal form of P3HT aggregates formed in solutions with different concentrations. UV-vis spectra of P3HT films spin-coated from isothermally crystallized solutions with different concentrations were obtained, and the results are shown in Fig. S6.[†] The P3HT films show optical absorption peaks at ~ 510 nm (0–2 absorption) corresponding to π – π absorption and at ~ 550 nm (0–1 absorption) and ~ 600 nm (0–0 absorption) corresponding to the shoulders of two vibronic absorption bands of P3HT in the solid state. Fig. S6[†] shows no redshift or blueshift phenomenon in the UV curves of P3HT films spin-coated from isothermally crystallized solutions that sheared at different temperatures. It was speculated that the FIP content has no effect on the conjugated length of the P3HT aggregates. The peak intensity of P3HT films increased with the FIP

content, indicating that the number of P3HT aggregates increased with the FIP content.

Effect of the shear rate on the shear-induced crystallization of P3HT in toluene

In addition to the shear temperature and the solution concentration, the shear rate is another important factor affecting the formation of FIPs and the crystallization of P3HT in toluene. To obtain a large FIP content to clearly observe the effect of the shear rate, we chose the most suitable shear temperature for PS_{0.2} and PS_{0.7} to be 60 °C and that for PS_{5.0} to be 80 °C, at which the FIP content was the largest under each concentration. Fig. 7 shows that an obvious absorption peak at ~ 607 nm appears in each sheared P3HT solution with different concentrations. The intensity of the absorption peak first increased with increasing shear rate, and then, the intensity decreased as the shear rate further increased. The most suitable shear rate to obtain the highest intensity of the absorption peak at ~ 607 nm varies with the solution concentration. For PS_{0.2,60}, the most suitable shear rate is 1.0 s^{−1}; for PS_{0.7,60}, the most suitable shear rate is 2.0 s^{−1}; and for PS_{5.0,80}, the most suitable shear rate is 3.0 s^{−1}. The absorption intensity is related to the FIP content. The above data indicate that the most suitable shear rate to obtain the highest FIP content increases with increasing solution concentration. A high shear rate is needed to form a large FIP content in the P3HT solution with a high concentration. In each P3HT solution, the shear time t_s is fixed, and the increase in the shear rate $\dot{\gamma}$ leads to increases in the shear strain γ and shear

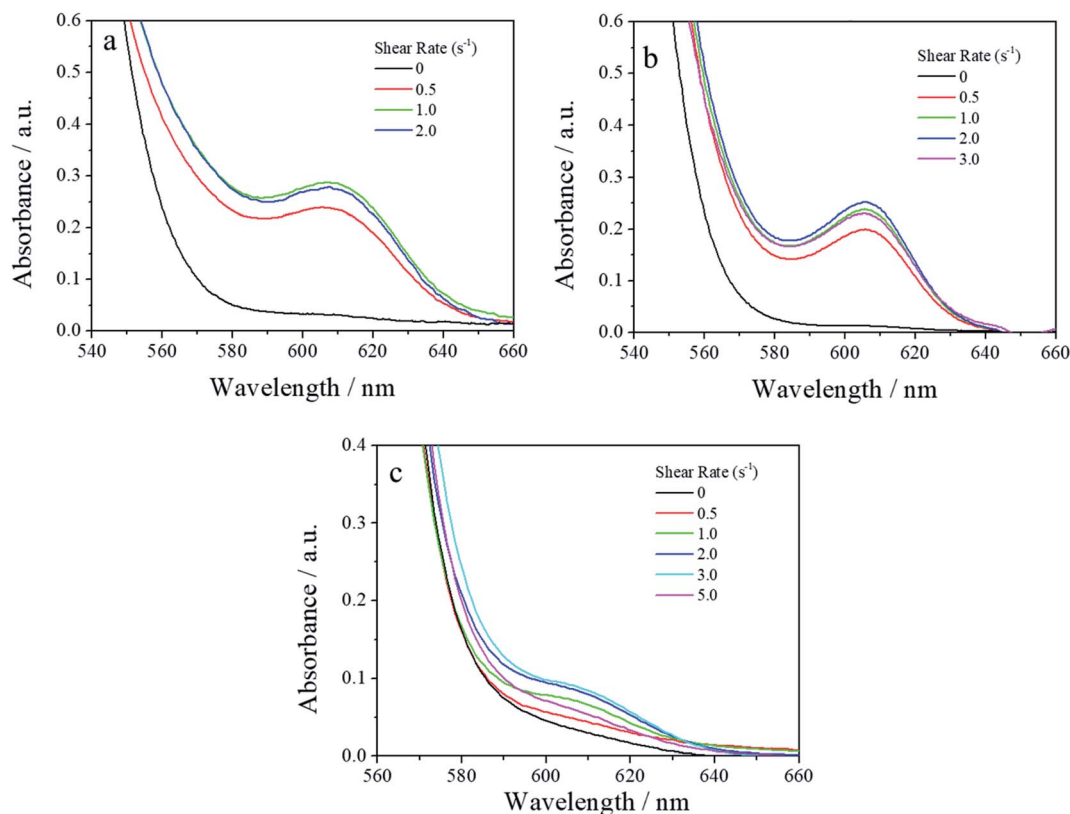


Fig. 7 UV-vis absorption spectra of (a) PS_{0.2,60}, (b) PS_{0.7,60} and (c) PS_{5.0,80} sheared at different shear rates.



stress σ . The effect of the shear rate $\dot{\gamma}$ on the crystallization of P3HT is evaluated by using the specific work (W). Janeschitz-Kriegl *et al.* reported that the nucleation rate is controlled by the specific mechanical work applied to a melt during shear, defined as⁴¹

$$W = \int_0^{t_s} \gamma \sigma dt = \sigma \gamma = \eta(\dot{\gamma}) \dot{\gamma}^2 t_s \quad (4)$$

The specific work W applied to the polymer during shear can be used to stretch polymer chains, and since W controls flow-induced crystallization, there is a proportional relation between W and the entropy reduction ΔS .³² During shear, not nearly all of the mechanical energy was consumed in stretching the polymer chains ($T_s \Delta S$) because of the energy dissipation caused by molecular friction and chain relaxation of the shorter chains. By introducing the dimensionless energy conversion factor E , the degree of entropy reduction can be simply derived with respect to W as³²

$$-T_s \Delta S = EW = E\eta(\dot{\gamma}) \dot{\gamma}^2 t_s \quad (5)$$

In the P3HT solution with a fixed concentration at the same shear temperature, the shear stress σ increases with the increase of the shear rate $\dot{\gamma}$, and first the FIP amount increases with the increase of σ . When σ exceeds the critical value, the formed FIPs were destroyed under the strong shear flow, and thus, the FIP amount decreases with the further increase of $\dot{\gamma}$. E is the energy conversion factor. Seo *et al.* investigated the shear-induced crystallization of poly(ether ether ketone) and found that $E = 0.011$. This result implies that only $\sim 1\%$ of the mechanical energy input reduces the entropy-relevant free energy due to the dominance of friction and relaxation effects.²⁷ In P3HT toluene solution, the high concentration solution has high viscosity, which may dissipate more mechanical energy under shear, namely, E is low in high concentration solution. To reduce the entropy to accelerate nucleation and crystallization, a higher W was needed. Therefore, the most suitable shear rate increases with increasing solution concentration to reduce the entropy. The reduction in entropy is related to the formation of FIPs, and thus, the most suitable shear rate increases with increasing solution concentration to obtain the highest amount of FIPs.

The effect of the shear rate $\dot{\gamma}$ on the crystallization kinetics of P3HT was investigated, and the results are shown in Fig. 8. Since the variation trend of the FIP content with $\dot{\gamma}$ was similar in each P3HT solution with different concentrations, PS_{0.2} is used as an example to investigate the crystallization kinetics (the crystallization rate of the dilute solution is relatively slow, and thus, the crystallization of P3HT between 6 °C and 12 °C can be studied in detail by using UV-vis spectroscopy). Fig. 8 shows that the G of P3HT increased with decreasing crystallization temperature when the solution was sheared at each shear rate. At the same crystallization temperature, the G of P3HT increased when the solution was sheared as the shear rate increased from 0.5 s⁻¹ to 1.0 s⁻¹ and then decreased slightly with further increases in the shear rate to 2.0 s⁻¹, indicating that the crystallization rate of P3HT was higher in sheared solutions with more FIPs.

UV-vis spectroscopy and GIXRD were used to investigate the effect of the shear rate on the number and structure of

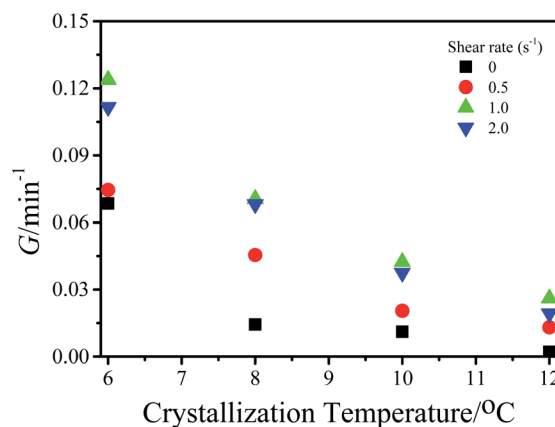


Fig. 8 Plots of the crystal growth rate versus crystallization temperature for PS_{0.2,60} sheared at different shear rates.

crystalline P3HT aggregates. Fig. S7a† shows that the absorption intensity of P3HT aggregates increased as the shear rate increased from 0.5 s⁻¹ to 1.0 s⁻¹ and then decreased with further increases in the shear rate to 2.0 s⁻¹, indicating that the largest number of P3HT aggregates formed in the solution sheared at a shear rate of 1.0 s⁻¹, verifying that a high FIP content improves the aggregation of P3HT in the solution. In Fig. S7b,† all P3HT aggregates show a (100) plane at $2\theta = 5.5^\circ$, indicating that the shear rate $\dot{\gamma}$ has no effects on the crystal form of P3HT nanofibres.

Conclusions

In this work, we investigate the microfluidic shear-induced formation of FIPs and the crystallization of P3HT in toluene and obtain the following results:

(1) The shear temperature, solution concentration and shear rate determine the FIP content. Upon fixing the shear rate and shear temperature, the FIP content increases as the solution concentration increases from 0.2 mg mL⁻¹ to 0.4 mg mL⁻¹ and then generally decreases with further increases in the solution concentration. Upon fixing the shear temperature, the most suitable shear rate at which the largest FIP content can be obtained increases with increasing solution concentration.

(2) The FIP content dramatically affects the crystallization of P3HT in toluene. Increasing the FIP content can accelerate the crystallization kinetics and change the crystallization mechanism from a second-order reaction to a first-order reaction of P3HT aggregates.

Conflicts of interest

There are no conflicts to declare.

Acknowledgements

This work is supported by the National Natural Science Foundation of China (Grant No. 21975029). A portion of this work is based on the data obtained at 1W1A, BSRF. The authors



gratefully acknowledge the assistance of the beamline scientists at Diffuse X-ray Scattering Station (1W1A), BSRF during the experiments.

Notes and references

- 1 B. O'Connor, R. Joseph Kline, B. R. Conrad, L. J. Richter, D. Gundlach, M. F. Toney and D. M. DeLongchamp, *Adv. Funct. Mater.*, 2011, **21**, 3697–3705.
- 2 S. E. Root, S. Savagatrup, A. D. Printz, D. Rodriguez and D. J. Lipomi, *Chem. Rev.*, 2017, **117**, 6467–6499.
- 3 Y. Park, J. W. Jung, H. Kang, J. Seth, Y. Kang and M. M. Sung, *Nano Lett.*, 2019, **19**, 1028–1032.
- 4 X. Zhang, N. Yuan, S. Ding, D. Wang, L. Li, W. Hu, Z. Bo, J. Zhou and H. Huo, *J. Mater. Chem. C*, 2017, **5**, 3983–3992.
- 5 X. Zhao, N. Yuan, Y. Zheng, D. Wang, L. Li, Z. Bo, J. Zhou and H. Huo, *Org. Electron.*, 2016, **28**, 189–196.
- 6 N. Yuan and H. Huo, *Nanotechnology*, 2016, **27**, 06LT01.
- 7 K. Vakhshouri and E. D. Gomez, *Macromol. Rapid Commun.*, 2012, **33**, 2133–2137.
- 8 J. A. Armas, K. J. Reynolds, Z. M. Marsh, M. Stefik, G. E. Scott and S. Zhang, *Macromol. Chem. Phys.*, 2018, **219**, 1800204.
- 9 X. Zhang, Y. Liu, X. Ma, H. Deng, Y. Zheng, F. Liu, J. Zhou, L. Li and H. Huo, *Soft Matter*, 2018, **14**, 3590–3600.
- 10 G. Qu, J. J. Kwok and Y. Diao, *Acc. Chem. Res.*, 2016, **49**, 2756–2764.
- 11 K. J. Ihn, J. Moulton and P. Smith, *J. Polym. Sci., Part B: Polym. Phys.*, 1993, **31**, 735–742.
- 12 J. J. Wie, N. A. Nguyen, C. D. Cwalina, J. Liu, D. C. Martin and M. E. Mackay, *Macromolecules*, 2014, **47**, 3343–3349.
- 13 G. Wang, N. Persson, P.-H. Chu, N. Kleinhenz, B. Fu, M. Chang, N. Deb, Y. Mao, H. Wang, M. A. Grover and E. Reichmanis, *ACS Nano*, 2015, **9**, 8220–8230.
- 14 M. Chang, Z. Su and E. Egar, *Macromolecules*, 2016, **49**, 9449–9456.
- 15 M. Chang, D. Choi and E. Egar, *ACS Appl. Mater. Interfaces*, 2016, **8**, 13484–13491.
- 16 Y. Liu, S. Hu, F. Liu, N. Wei, J. Zhou, L. Li and H. Huo, *Polym. Cryst.*, 2020, **3**, e10093.
- 17 H. An, B. Zhao, Z. Ma, C. Shao, X. Wang, Y. Fang, L. Li and Z. Li, *Macromolecules*, 2007, **40**, 4740–4743.
- 18 Y. Geng, G. Wang, Y. Cong, L. Bai, L. Li and C. Yang, *Macromolecules*, 2009, **42**, 4751–4757.
- 19 K. Cui, Z. Ma, N. Tian, F. Su, D. Liu and L. Li, *Chem. Rev.*, 2018, **118**, 1840–1886.
- 20 X. Tang, J. Yang, F. Tian, T. Xu, C. Xie, W. Chen and L. Li, *J. Chem. Phys.*, 2018, **149**, 224901.
- 21 W. Chen, Q. Zhang and L. Li, *J. Appl. Phys.*, 2020, **127**, 241101.
- 22 L. Balzano, N. Kukalyekar, S. Rastogi, G. W. Peters and J. Chadwick, *Phys. Rev. Lett.*, 2008, **100**, 048302.
- 23 B. Hsiao, L. Yang, R. Somani, C. Avila-Orta and L. Zhu, *Phys. Rev. Lett.*, 2005, **94**, 117802.
- 24 Y. Luo, F. A. Santos, T. W. Wanger, E. Tsoi and S. Zhang, *J. Phys. Chem. B*, 2014, **118**, 6038.
- 25 T. W. Wanger, Y. Luo, N. D. Redeker, C. E. Immoos and S. Zhang, *Polymer*, 2014, **55**, 2008.
- 26 M. M. Bouman, E. E. Havinga, R. A. J. Janssen and E. W. Meijer, *Mol. Cryst. Liq. Cryst.*, 1994, **256**, 439–448.
- 27 J. Seo, A. M. Gohn, R. P. Schaake, D. Parisi, A. M. Rhoades and R. H. Colby, *Macromolecules*, 2020, **53**, 3472–3481.
- 28 P. J. Flory, *J. Chem. Phys.*, 1947, **15**, 397–408.
- 29 P. J. Flory, *J. Chem. Phys.*, 1949, **17**, 223–240.
- 30 J. D. Hoffman and J. Lauritzen, *J. Res. Natl. Bur. Stand., Sect. A*, 1961, **65**, 297–336.
- 31 A. J. McHugh, *Polym. Eng. Sci.*, 1982, **22**, 15–26.
- 32 J. D. Hoffman, C. M. Guttman and E. A. Dimarzio, *Faraday Discuss.*, 1979, **68**, 177–197.
- 33 B. Nazari, H. Tran, B. Beauregard, M. Flynn-Hepford, D. Harrell, S. T. Milner and R. H. Colby, *Macromolecules*, 2018, **51**, 4750–4761.
- 34 O. O. Mykhaylyk, P. Chambon, C. Impraham, J. P. A. Fairclough, P. D. Olmsted and A. J. Ryan, *Macromolecules*, 2008, **41**, 1901–1904.
- 35 O. O. Mykhaylyk, P. Chambon, C. Impradice, J. P. A. Fairclough, N. J. Terrill and A. J. Ryan, *Macromolecules*, 2010, **43**, 2389–2405.
- 36 K. Cui, L. Meng, Y. Ji, J. Li, S. Zhu, X. Li, N. Tian, D. Liu and L. Li, *Macromolecules*, 2014, **47**, 677–686.
- 37 N. Ding and E. J. Amis, *Macromolecules*, 1991, **24**, 6464–6469.
- 38 D. W. Bilger, J. A. Figueroa, N. D. Redeker, A. Sarkar, M. Stefik and S. Zhang, *ACS Omega*, 2017, **2**, 8526–8535.
- 39 C. D. Danesh, N. S. Starkweather and S. Zhang, *J. Phys. Chem. B*, 2012, **116**, 12887–12894.
- 40 A. P. Philipse and A. M. Wierenga, *Langmuir*, 1998, **14**, 49–54.
- 41 H. Janeschitz-Kriegl, E. Ratajski and M. Stadlbauer, *Rheol. Acta*, 2003, **42**, 355–364.

